Double-Layer Interaction between Two Parallel Rodlike Objects Partially Immersed in an Oil/Water Interface

Jyh-Ping Hsu* and Bo-Tau Liu

Department of Chemical Engineering, National Taiwan University, Taipei, Taiwan 10617, Republic of China

Received: November 25, 1996; In Final Form: March 24, 1997[⊗]

The electrical double-layer interaction between two long, parallel rodlike objects partially immersed in a water/oil interface is analyzed. The present approach is applicable to a system containing two different objects. A family of shapes formed by deforming a cylinder is considered through a conformal mapping technique. An analytical expression for the electrical potential distribution for the system under consideration is derived under the Debye−Huckle condition. We show that the thicker the electrical double layer, the greater the interaction free energy and the stabler the system. For a fixed thickness of electrical double layer, the closer the objects to cylinders and/or the smaller the contact angle (the larger the fraction of an object in the water phase), the stable the system. Also, the greater the difference in the charged conditions on the two interaction objects, the stabler the system. If the deviation in the contact angle is close to $\pi/2$, the interaction free energy is roughly a linear function of the position of the water/oil interface.

Introduction

It is known that finely dispersed particles over a liquid−liquid interface can serve as an efficient emulsion-stabilizing agent.[1] This phenomenon has the potential of various applications in practice. In some cases reducing the stability of an emulsion system is of major concern. A typical example is the water-in-oil emulsion formed in enhanced oil recovery operations. In this case, since it may create various problems,[2] the formation of water droplets is disadvantageous to the operations. On the other hand, searching for an effective stabilizing agent becomes essential in numerous food and cosmetic industries. Water-in-oil microemulsions can be used to produce namometer-sized metal and semiconductor particles. Here, the dispersed water droplets, stabilized by surfactant molecules near the water/oil interface, serve as microreactors in which chemical reactions occur.[3] Tadros and Vincent[4] concluded that an emulsion system is stabler if it has a smaller particle size, rougher particle surface, and an appropriate contact angle formed between the liquid−liquid interface and the particle surface. Denkov et al.[4] suggested that these experimental findings can be explained by considering a mechanism which takes into account the effect of contact angle hysteresis on the effective disjoining pressure isotherms. Apparently, the nature of the stabilizing agent plays a significant role here. In a study of the electrical interaction force between two objects immersed in an oil/water interface, Lyne et al.[6] considered the case of two identical, infinitely long, parallel cylinders and a symmetric electrolyte solution. The governing equations were solved numerically. It was found that there are a short-range double-layer repulsion force between cylinders acting through the electrolyte medium and a relative long-range repulsion force acting through the oil medium.

In practice, the dispersed particles may not have the same physical properties. Polydispersity, for example, is one of the key problems which needs to be considered. The deviations in the geometries and the surface conditions of the dispersed particles are also not uncommon and should be taken into account in the simulation of industrial operations. The former may due to, for example, the influence of various external forces acting on the particles, and the latter arises from the variations in the local physicochemical properties of the liquid phases. A systematic approach which takes these factors into account is highly desirable. In the present study, the analysis of Lyne et al.[5] is extended to the case of two rodlike objects. The shapes of these objects and their surface conditions can be different, and a family of shapes formed by deforming a cylinder is taken into account.

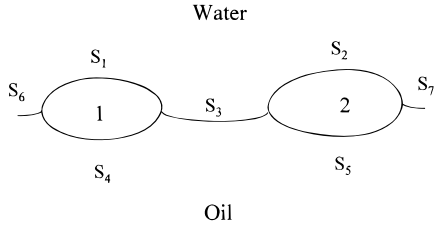

Figure 1. Cross-sectional view of the system under consideration for the case of horizontally oriented objects. Objects 1 and 2 are two infinitely long, parallel, rodlike solid objects, S_1 and S_2 the water/solid interfaces, S_3, S_6, and S_7 the water/oil interfaces and S_4 and S_5 the oil/solid interfaces.

Modeling

By referring to Figure 1, we consider two long, parallel, rodlike solid objects partially immersed in an oil/water interface. These objects lie flat on the interface. Suppose that the surfaces of the objects in the water phase (S_1 and S_2) are charged, and those in the oil phase (S_4 and S_5) are free of charges. Since the dielectric constant of water is about 30−40 times greater than than of oil,[2,7] the electrical potential distribution in the oil phase is not considered. This will not, in general, cause too much deviation in the evaluation of the electrostatic interactions between two objects.[6] The water phase is an electrolyte solution, and double layers are formed near S_1 and S_2. If S_1 and S_2 are not highly charged, the electrical potential distribution in the water phase can be described, approximately, by the linearized Poisson−Boltzmann equation[8,9]

* To whom correspondence should be addressed. Fax: 886-2-3623040. E-mail: T8504009@ccms.ntu.edu.tw.

[⊗] Abstract published in *Advance ACS Abstracts,* May 1, 1997.

S1089-5647(96)03917-X CCC: $14.00 © 1997 American Chemical Society

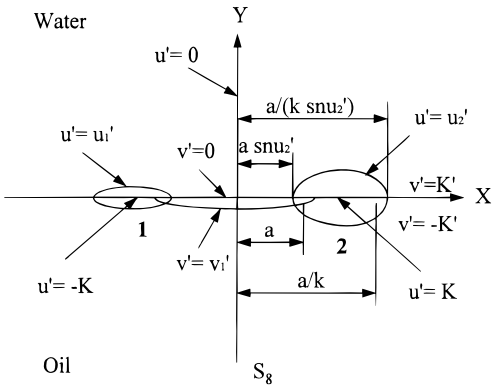

Figure 2. Schematic representation of sn-cylinder coordinates. S_8 is the midplane between two objects.

$$\Delta y = \kappa^2 y \tag{1}$$

where

$$y = e\psi/k_B T \tag{1a}$$

$$\kappa^2 = 8\pi e^2 I/\epsilon k_B T \tag{1b}$$

In these expressions, Δ denotes the Laplace operator, ϵ the dielectric constant, ψ the electrical potential, e and I the elementary charge and the ionic strength, respectively, T the absolute temperature, and κ and k_B the reciprocal Debye length and the Boltzmann constant, respectively. Let us consider the transformation[10,11]

$$z = X + iY = a\cdot\mathrm{sn}(w) = a\cdot\mathrm{sn}(u'+iv') \tag{2}$$

where sn denotes the Jacobi elliptic function (Appendix A). This is a conformal mapping which maps the coordinates X and Y of the Cartesian coordinates $\{X,Y,Z\}$ to coordinates u' and v'. This technique provides a useful tool for transforming a domain into another one having some desirable nature.[12] For example, an orthogonal coordinate system still reduces to another orthogonal coordinate after the transformation. In the present case, the rodlike geometry in the (X,Y) plane can be simulated by a simple geometry in the (u',v') plane. By referring to Figure 2, a is the distance between the midplane S_8 and the focus of an object. The transformation defined by (2) maps the domain $-\infty < X < \infty$ and $-\infty < Y < \infty$ to $-K < u' < K$ and $-K' < v' < K'$, where K and K' are, respectively, the complete elliptic integral of the first kind with parameters k and k', $k' = (1 - k^2)^{1/2}$. The water/solid interfaces S_1 and S_2 are described by $u' = u_1'$ and $u' = u_2'$, respectively, and the water/oil interface S_3 by $v' = v_1'$. The value of v_1' is characterized by the contact angle at the solid/water/oil interface. Note that if $k \to 0$, $u' =$ constant represents a cylindrical surface; otherwise, it describes an oval-shaped surface. We assume that the water/oil interfaces are uncharged, the electrical potential vanishes deep in the water phase, and the water/solid interfaces remain at constant electrical potential. Therefore, in terms of the notations shown in Figure 1, the boundary conditions associated with (1) are

$$\frac{\partial y}{\partial n} = 0, \quad \text{at } S_3, S_6, \text{ and } S_7 \tag{3a}$$

$$y = 0, \quad \text{deep in water phase} \tag{3b}$$

$$y = y_1, \quad \text{at } S_1 \tag{3c}$$

$$y = y_2, \quad \text{at } S_2 \tag{3d}$$

where n denotes the outer normal of a surface and y_1 and y_2 are the dimensionless surface potentials of S_1 and S_2, respectively.

If we denote G as the Green function[13] of the boundary value problem defined by (1), and (3a), and (3b), the solution to (1) can be expressed as

$$y\int_s (y_s\cdot G_n)\mathrm{dS} + \kappa^2\int_v (G\cdot y)\mathrm{dV} \tag{4}$$

where G_n is the derivative of G with respect to n. The surface integral (first term) on the right-hand side of (4) denotes the effect of the nonhomogeneous boundary conditions, and the volume integral (second term) represents a source effect. Since the electrical potential distribution is independent of the Z coordinate, a unit length in the Z direction is chosen in performing the integrations of the right-hand side of (4), for convenience. As illustrated in Appendix B, the appropriate Green function is

$$G(u,v|\xi,\eta) = -L_u\cdot L_v\sum_{m=0}^{\infty}\sum_{n=1}^{\infty} w\frac{\cos\left(\frac{m\pi}{L_v}v\right)\sin\left(\frac{n\pi}{L_u}u\right)\cos\left(\frac{m\pi}{L_v}\eta\right)\sin\left(\frac{n\pi}{L_u}\xi\right)}{\pi^2(m^2 L_u^{\,2} + n^2 L_v^{\,2})} \tag{5}$$

where w is 2 if $m = 0$ and 4 if $m \neq 0$, $u = u' - u_1'$, $v = v' - v_1'$, $L_u = u_2' - u_1'$, and $L_v = v_2' - v_1'$. Substituting (5) into (4) yields

$$y(u,v) = \frac{y_2 - y_1}{L_u}u + y_1 + \kappa^2\int_0^{L_v}\int_0^{L_u} G(u,v|\xi,\eta)\, y(\xi,\eta)\, g_1(\xi,\eta)\, \mathrm{d}\xi\, \mathrm{d}\eta \tag{6}$$

where

$$g_1 = \frac{a^2\Omega^2}{\Lambda^2} \tag{6a}$$

and

$$\Omega^2 = (1 - \mathrm{sn}^2(u')\cdot\mathrm{dn}^2(v'))\cdot(\mathrm{dn}^2(v') - k^2\,\mathrm{sn}^2(u')) \tag{6b}$$

$$\Lambda = 1 - \mathrm{dn}^2(u')\cdot\mathrm{sn}^2(v') \tag{6c}$$

Here, g_1 is the metric coefficient. (6) is the Fredholm equation of the second kind,[14] which can be rewritten as

$$y(u,v) = B - c^2\sum_{m=0}^{\infty}\sum_{n=1}^{\infty}\lambda_{mn}\int_0^{L_v}\int_0^{L_u}\Phi_{mn}(u,v)\,\Phi_{mn}(\xi,\eta)\,h^2(\xi,\eta)y\,\mathrm{d}\xi\,\mathrm{d}\eta \tag{7}$$

where

$$B = \frac{y_2 - y_1}{L_u}u + y_1 \tag{7a}$$

$$c = \kappa a \tag{7b}$$

$$\lambda_{mn} = \frac{L_u L_v}{\pi^2} \frac{w}{m^2 L_u^2 + n^2 L_v^2}, \quad m = 0, 1, ..., \quad n = 1, 2, ... \tag{7c}$$

$$\Phi_{mn}(\xi,\eta) = \sin\left(\frac{n\pi}{L_u}\xi\right)\cos\left(\frac{m\pi}{L_v}\eta\right), \quad m = 0, 1, ..., \quad n = 1, 2, ... \tag{7d}$$

$$h = \Omega/\Lambda \tag{7e}$$

Multiplying $\Phi_{mn}(u,v)h^2$ on both sides of (7) and integrating the resultant expression from 0 to L_u for u and from 0 to L_v for v, we obtain

$$\mathbf{C} = (\mathbf{I} + c^2\mathbf{M})'\mathbf{P} \tag{8}$$

where **I** is identity matrix and the elements of matrices **C**, **M**, and **P** are

$$c_i = c_{mn} \tag{8a}$$

$$M_{ij} = \lambda_{m'n'} \cdot M_{mn,m'n'} \tag{8b}$$

$$P_i = P_{mn} \tag{8c}$$

with $m, m' = 0, 1, 2, ...,$ $n, n' = 1, 2, 3, ...,$ and

$$P_{mn} = \int_0^{L_v}\int_0^{L_u} B\Phi_{mn}(u,v)\, h^2(u,v)\, du\, dv \tag{9a}$$

$$c_{mn} = \int_0^{L_v}\int_0^{L_u} \Phi_{mn}(\xi,\eta)\, y(\xi,\eta)\, h^2(\xi,\eta)\, d\xi\, d\eta \tag{9b}$$

$$M_{mn,m'n'} = \int_0^{L_v}\int_0^{L_u} \Phi_{mn}(u,v)\, \Phi_{m'n'}(u,v)\, h^2\, du\, dv \tag{9c}$$

The solution to (1) is then

$$y(u,v) = F(u,v) - c^2\sum_{m=0}^{\infty}\sum_{n=1}^{\infty}\lambda_{mn}c_{mn}\Phi_{mn}(u,v) \tag{10}$$

The dimensionless Helmholtz free energy for a system containing a single charged surface can be evaluated by[15]

$$f = -\frac{1}{2}y_1\int_{s_1}\sigma_1\, ds - \frac{1}{2}y_2\int_{s_2}\sigma_2\, ds \tag{11}$$

The dimensionless surface charge density, σ, can be determined on the basis of the Gauss's law as

$$\vec{n}\cdot\vec{\nabla}y = \frac{4\pi e\sigma'}{\epsilon k_B T} = \frac{\sigma}{a} \tag{12}$$

where σ' is surface charge per unit area. Substituting (10) and (12) into (11) yields

$$f = -\frac{(y_1 - y_2)^2 L_v}{2L_u} - \frac{y_1 c^2}{2}\sum_{n=1}^{\infty}\lambda_{0n}C_{0n}\frac{n\pi L_v}{L_u} + \frac{y_2 c^2}{2}\sum_{n=1}^{\infty}\lambda_{0n}C_{0n}(-1)^n\frac{n\pi L_v}{L_u} \tag{13}$$

The electrical repulsive force between two objects can be calculated by[16]

$$F = \int_{S_8}\left[\left(\Delta\pi + \frac{\epsilon E^2}{8\pi}\right)\vec{n} - \frac{\epsilon}{4\pi}(\vec{E}\cdot\vec{n})\vec{E}\right]ds \tag{14}$$

where S_8 is the midplane between objects 1 and 2 represented by $u' = 0$, as shown in Figure 2, $\vec{E}$ the electrical field vector with strength E, and $\Delta\pi$ the osmotic pressure. If ψ is low over S_8, then[16]

$$\Delta\pi = \frac{\epsilon\kappa^2}{8\pi}\psi^2 \tag{15}$$

Substituting (10) to (14) gives

$$F^* = \int_{-K'}^{K'}\left[c^2 y^2 h + \frac{E_v^{*2} - E_u^{*2}}{h}\right]dv \tag{16}$$

where the dimensionless electrical repulsive force, F^*, is defined by $F^* = 8\pi e^2 F/\epsilon k_B^2 T^2$ and

$$-E_u^* = \frac{y_2 - y_1}{L_u} - c^2\sum_{m=0}^{\infty}\sum_{n=1}^{\infty}\frac{n\pi}{L_u}\lambda_{mn}c_{mn}\cos\left(\frac{n\pi}{L_u}u\right)\cos\left(\frac{m\pi}{L_v}v\right) \tag{17a}$$

$$-E_v^* = c^2\sum_{m=0}^{\infty}\sum_{n=1}^{\infty}\frac{m\pi}{L_v}\lambda_{mn}c_{mn}\sin\left(\frac{n\pi}{L_u}u\right)\sin\left(\frac{m\pi}{L_v}v\right) \tag{17b}$$

Results and Discussion

A more rigorous description for the boundary condition at the oil/water interface can be expressed as

$$\epsilon_w\frac{\partial y}{\partial n} - \epsilon_o\frac{\partial y}{\partial n} = -4\pi\sigma_{w/o} \tag{18}$$

where ϵ_w and ϵ_o are, respectively, the dielectric constants of water and oil and $\sigma_{w/o}$ is the charge density on the water side of the oil/water interface. Since $\epsilon_w \gg \epsilon_o$ under typical conditions, the second term on the left-hand side of (18) can be neglected. Furthermore, if ϵ_w is sufficiently large, it reduces to (3a). The contribution due to the presence of the oil phase is neglected in the evaluation of the electrical interaction force. This is usually satisfactory.[8] For the special cases in which the oil phase needs to be considered, the present analysis can be adopted to estimate the boundary condition for the oil side of the oil/water interface first, and the governing equations are then solved for the oil phase.

Figure 3 shows the simulated electrical potential distribution for the case of two rodlike objects. Note that (2) transforms the infinite region ($X \rightarrow \pm\infty$, $Y \rightarrow -\infty$) to ($u' = 0$, $v' = K'$) and ($X \rightarrow \pm\infty$, $Y \rightarrow \infty$) to ($u' = 0$, $v' = K'$), respectively. As can be seen from this figure, the electrical potential vanishes at ($u' = 0$, $v' = K' = 2.8$). This is consistent with (3b).

If the value of $a\cdot\mathrm{sn}(u)$ is fixed, $c\cdot\mathrm{sn}(u)$ varies with κ, the inverse thickness of the electrical double layer; the smaller the former, the smaller the latter. For an easier presentation, we define the dimensionless force based on the surface potential, F^{**}, as

$$F^{**} = F^*/y_1^2 \tag{19}$$

Figure 4 shows the variation of F^{**} as a function of $c\cdot\mathrm{sn}(u)$. This figure reveals that the smaller the value of $c\cdot\mathrm{sn}(u)$, the greater the interaction force between two objects. That is, the thicker the electrical double layer, the greater the interaction free energy. This is consistent with the result of Lyne et al.[8] Therefore, reducing the concentration of electrolyte in the water

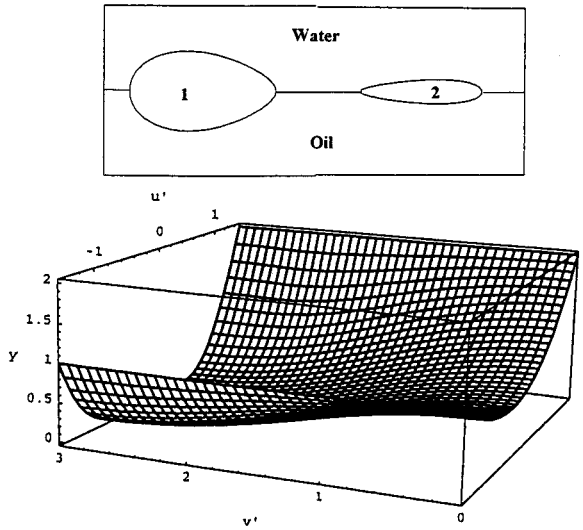

Figure 3. Electrical potential distribution for the case $k = 0.25$, $v_1' = 0$, $u_1' = -1.117\ 39$, $u_2' = 1.436\ 618$, $y_2/y_1 = 2$, and $c\cdot\mathrm{sn}(u_2) = 1$.

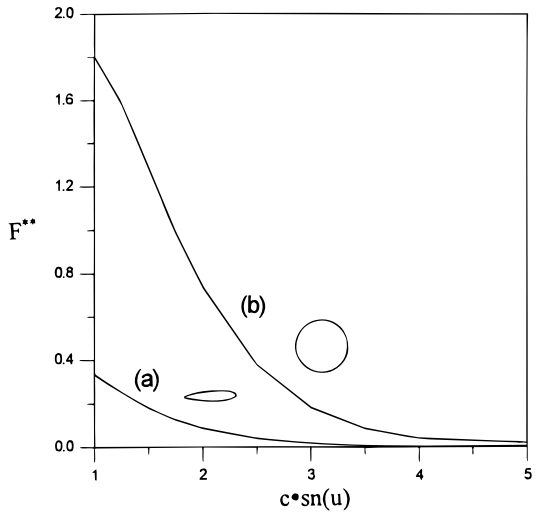

Figure 4. Variation of the electrical interaction force between two objects as a function of the thickness of the electric double layer for the case $y_2/y_1 = 2$ and $u_1 = u_2$. (a) $a = 1$, $k = 0.25$, and $u_2 = 1.436\ 618$; (b) $a = 1.897\ 367$, $k = 0.9$, and $u_2 = 0.571\ 063\ 4$.

phase has the effect of increasing the stability of the system under consideration. Note that, however, if the electrical double layer is too thick, it is possible that the electrical repulsion force between adjacent particles may induce some instability. Figure 4 also suggests that, for a fixed thickness of electrical double layer and the same longest diameter of an object, the more the object deviates from a cylinder, the smaller the interaction force. A more detailed illustration for the effect of the shape of an object, measured by the parameter k, on the dimensionless interaction force F^{**} is shown in Figure 5. This figure reveals that the greater the k (the closer to a cylinder), the greater the F^{**} and the stabler the system. The rate of increase of F^{**} as k varies, however, decreases with the increase in k.

The effect of the contact angle, measured by the position of the water/oil interface (v_1' = constant), on the interaction free energy between two objects is presented in Figure 6. As can be seen from this figure, the smaller the contact angle (the smaller the value of v_1', or the larger the fraction of an object in the water phase), the greater the interaction free energy between two objects and the stabler the system. Note that if the contact angle is close to $\pi/2$ ($v_1' \approx 0$), the variation of the interaction free energy as a function of the position of water/oil interface is roughly linear.

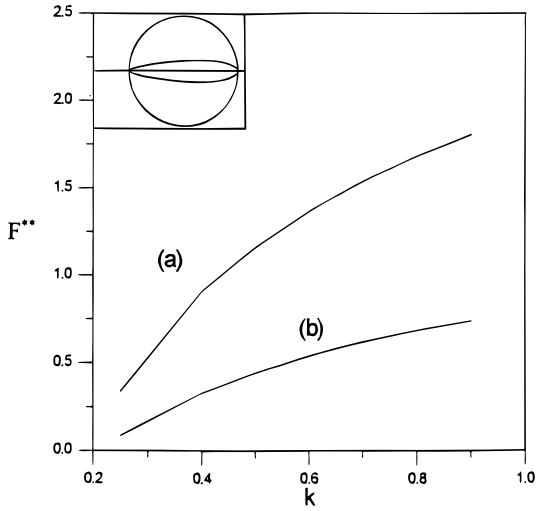

Figure 5. Variation of the electrical interaction force between two objects as a function of k for the case $y_2/y_1 = 2$ and $u_1 = u_2$. (a) $c\cdot\mathrm{sn}(u) = 1$; (b) $c\cdot\mathrm{sn}(u) = 2$. Inset: the deformed proceeding is shown in the upper left-hand side of the figure.

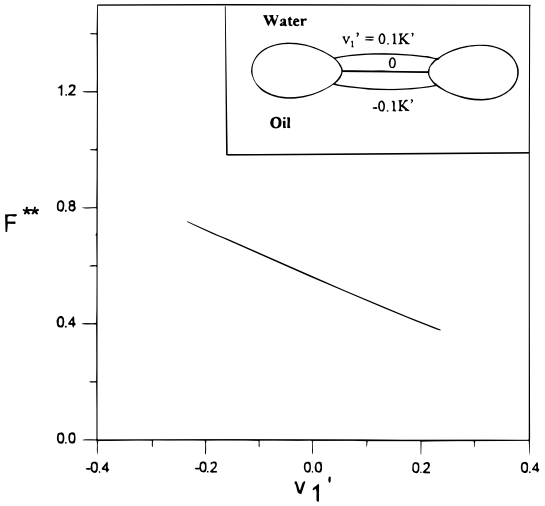

Figure 6. Variation of the interaction electrical force between two objects as a function of v_1' for the case $a = 0.5$, $k = 0.4$, $u_1' = 0.7K$, $u_2' = -u_1'$, $y_2/y_1 = 2$, and $c\cdot\mathrm{sn}(u) = 1$.

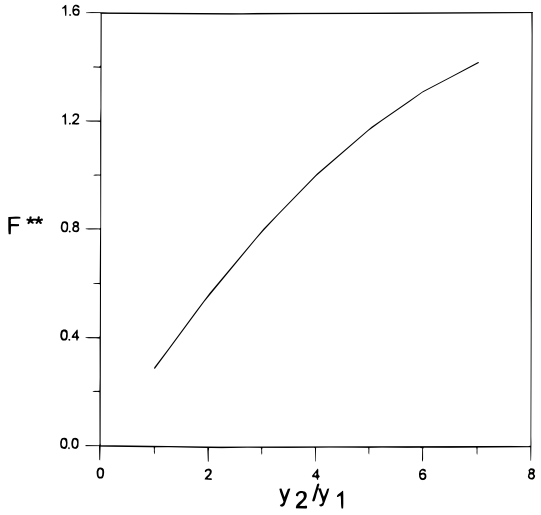

Figure 7. Variation of the electrical interaction force between two surfaces as a function of y_2/y_1 for the case of Figure 5.

Figure 7 illustrates the variation in the interaction force between two objects as a function of the ratio y_2/y_1 (dimension-

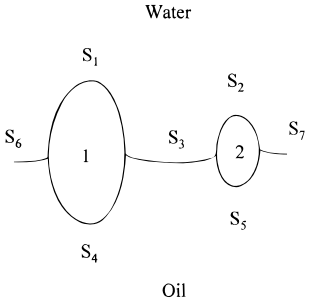

Figure 8. Cross-sectional view of the system under consideration for the case of vertically oriented objects.

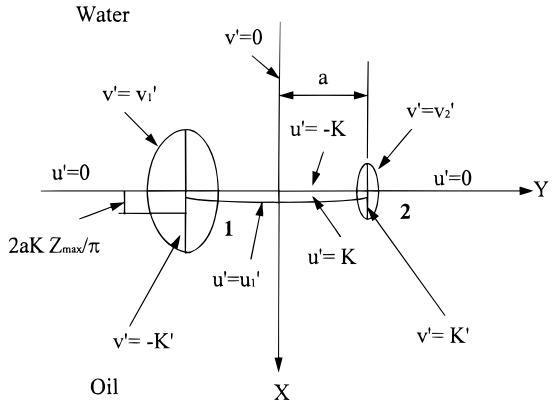

Figure 9. Schematic representation of ζ-cylinder coordinates.

less surface potential of object 2/dimensionless surface potential of object 1). This figure indicates that the greater the difference in the charged conditions on the two interaction objects, the greater the interaction force and the stabler the system under consideration.

As suggested by (13), even if one of the two objects is free of charges, the interaction free energy between two objects does not vanish. This is because although the electrical repulsion energy between two objects vanishes, the contribution due to the osmotic pressure still exists (Appendix C).

Suppose that the relative orientation of the two interacting objects is shown in Figure 8. In this case we define the transformation[9,10]

$$\bar{z} = \frac{2Ka}{\pi}\zeta(w+iK) + ia \tag{20}$$

where ζ is the Riemann zeta function. This leads to the coordinates presented in Figure 9. The metric coefficient, (6a), becomes

$$g_1 = \left(\frac{2Ka}{\pi}\right)^2\left\{\frac{4k^4}{\Lambda'^4}\mathrm{sn}^2(u')\cdot\mathrm{cn}^2(u')\cdot\mathrm{dn}^2(u')\cdot\mathrm{sn}^2(v'+K')\cdot \mathrm{cn}^2(v'+K')\cdot\mathrm{dn}^2(v'+K) + \left[\mathrm{dn}^2(u') - \frac{E}{K} + \frac{k^2\,\mathrm{sn}^2(v'+K')}{\Lambda'^2}\times (\mathrm{dn}^2(u')\cdot cn^2(v'+K')(\mathrm{cn}^2(u') - \mathrm{sn}^2(u')\cdot\mathrm{dn}^2(u')) - k^2\mathrm{sn}^2(u')\cdot(1-k^2\mathrm{sn}^4(u'))\right]^2\right\} \tag{21}$$

with

$$\Lambda' = 1 - \mathrm{dn}^2(u')\cdot\mathrm{sn}^2(v'+K') \tag{21a}$$

$$E = \int_0^{\pi/2}\sqrt{1-k^2\sin^2\theta}\,\mathrm{d}\theta \tag{21b}$$

where E is the complete elliptic integral of the second kind.

The electrical potential distribution and the corresponding interaction force are described by (7) and (16), respectively.

In summary, the present conformal mapping technique is capable of providing a systematic way for describing the interaction between two objects of different geometries and surface conditions. This is highly desirable since the interacting objects may assume various shapes under the influence of various external forces such as surface tension and electrostatic force.

Acknowledgment. This work was supported by the National Science Council of the Republic of China.

Appendix A

Incomplete elliptic integral of the first kind for variable u' is defined as

$$u' = \mathrm{fn}(\varpi,k) = \int_0^{\varpi}\frac{\mathrm{d}\theta}{\sqrt{1-k^2\sin^2\theta}}, \quad -K < u' < K = \int_0^{\pi/2}\frac{\mathrm{d}\theta}{\sqrt{1-k^2\sin^2\theta}} \tag{A1}$$

The Jacobi elliptic functions are defined as

$$\mathrm{sn}(u') = \sin\varpi \tag{A2a}$$

$$\mathrm{dn}(u') = \sqrt{1-k^2\,\mathrm{sn}^2(u')} \tag{A2b}$$

The incomplete elliptic integral of the first kind for variable v' is obtained by replacing k with k' in (Al). We have

$$v' = \mathrm{fn}(\varpi,k') \tag{A3}$$

Under the present coordinate system the relative position and the sizes of the objects are determined by the parameters a, k, u_1', and u_2'. If $u' \to 0$, an object is planar; if $u' \to K$, it becomes a strip. If $k \to 1$, $u =$ constant represents a cylindrical surface with center at $(a(\mathrm{sn}(u') + 1/\mathrm{sn}(u'))/2, 0)$ and radius $a(1/\mathrm{sn}(u') - \mathrm{sn}(u'))/2$, as illustrated in Figure 2. The nearest and the farthest distances between an object and the midplane S_8 are $a\cdot\mathrm{sn}(u)$ and $a/(k\cdot\mathrm{sn}(u))$, respectively.

Appendix B

The auxiliary problem to (1) in terms of the Green's function is

$$\frac{\partial^2 G}{\partial u^2} + \frac{\partial^2 G}{\partial v^2} = \delta(u-\xi,v-\eta) \tag{B1}$$

The corresponding boundary conditions are

$$\frac{\partial G}{\partial n} = 0 \quad \text{at} \quad v = 0 \quad \text{and} \quad v = L_v \tag{B1a}$$

$$G = 0 \quad \text{at} \quad u = 0 \quad \text{and} \quad u = L_u \tag{B1b}$$

where δ is the delta function and

$$\int\int\delta(u-\xi,v-\eta)\,\mathrm{d}\xi\,\mathrm{d}\eta = 1 \tag{B1c}$$

The eigenvalue problem corresponding to (B1) is

$$\frac{\partial^2 G}{\partial u^2} + \frac{\partial^2 G}{\partial v^2} = -\lambda G \tag{B2}$$

with the homogeneous boundary conditions (B1a) and (B1b).

It can be shown that the eigenvalues and the eigenfunctions are (7c) and (7d), respectively. Expanding G and δ in terms of these eigenfunctions, we have

$$G(u,v|\xi,\eta) = \sum_m \sum_n a_{mn}(u,v)\, \Phi_{mn}(\xi,\eta) \tag{B3}$$

$$\delta(u-\xi,v-\eta) = \sum_m \sum_n \frac{\Phi_{mn}(u,v)}{\langle \Phi_{mn},\Phi_{mn}\rangle} \Phi_{mn}(\xi,\eta) \tag{B4}$$

where the inner product $\langle \Phi_{mn},\Phi_{mn}\rangle$ is defined as

$$\langle \Phi_{mn},\Phi_{mn}\rangle = \int\int_\Omega \Phi_{mn}\cdot\Phi_{mn}\, d\xi\, d\eta \tag{B4a}$$

Substituting (B3) and (B4) into (B1) and employing the relation between the eigenfunctions of (B2), (5) can be recovered.

Appendix C

Suppose that one of the two objects, say, object 2, is free of charges. In this case (B1a) and (B1b) become, respectively,

$$\frac{\partial G}{\partial n} = 0 \quad \text{at} \quad v = 0, \quad v = L_v, \quad \text{and } u = L_u \tag{C1a}$$

and

$$G = 0 \quad \text{at} \quad u = 0 \tag{C1b}$$

The corresponding Green function, eigenvalues, and eigenfunctions are, respectively,

$$-L_u\cdot L_v \sum_{m=0}^{\infty}\sum_{n=1}^{\infty} w \times \frac{\cos\left(\frac{m\pi}{L_v}v\right)\sin\left(\frac{(n-0.5)\pi}{L_u}u\right)\cos\left(\frac{m\pi}{L_v}\eta\right)\sin\left(\frac{(n-0.5)\pi}{L_u}\xi\right)}{\pi^2(m^2L_u^{\,2} + (n-0.5)^2L_v^{\,2})} \tag{C2a}$$

$$\lambda_{mn} = \frac{L_uL_v}{\pi^2}\frac{w}{m^2L_u^{\,2} + (n-0.5)^2L_v^{\,2}} \tag{C2b}$$

and

$$\Phi_{mn}(\xi,\eta) = \cos\left(\frac{m\pi}{L_v}\xi\right)\sin\left(\frac{(n-0.5)\pi}{L_u}\eta\right) \tag{C2c}$$

Following the same procedure as that employed in the derivation of (10), we obtain

$$y^1 = y_1 - c^2\sum_{m=0}^{\infty}\sum_{n=1}^{\infty}\lambda_{mn}^1 c_{mn}^1 \Phi_{mn} \tag{C3}$$

Substituting (C3) into (11), the free energy is

$$f = -\frac{y_1c^2}{2}\sum_{n=1}^{\infty}\lambda_{0n}^1 C_{0n}^1 \frac{(n-0.5)\pi L_v}{L_u} \tag{C4}$$

Since both C_{0n}^1 and L_v are functions of the position of object 2, the free energy is a function of the relative position of the interacting objects.

References and Notes

(1) Pickering, S. U. *J. Chem. Soc.* **1907**, *91*, 2001.
(2) Friesen, W. I.; Levine, S. *J. Colloid Interface Sci.* **1992**, *150*, 517.
(3) Fendler, J. H. *Chem. Rev.* **1987**, *87*, 877.
(4) Tadros, Th.V.; Vincent, B. *Encyclopedia of Emulsion Technology*; Becher, P., Ed.; Marcel Dekker: New York, 1983; Vol. 1, p 129.
(5) Denkov, N. D.; Ivanov, I. B.; Kralchevsky, P. A.; Wasan, D. T. *J. Colloid Interface Sci.* **1992**, *150*, 589.
(6) Lyne, M. P.; Bowen, B. D.; Levine, S. *J. Colloid Interface Sci.* **1992**, *150*, 374.
(7) Perry, R. H.; Green, D. W.; Maloney, J. O. *Perry's Chemical Engineers Handbook*, 6th ed.; McGraw-Hill: New York, 1984.
(8) Hiemenz, P. C. *Principles of Colloid and Surface Chemistry*, 2nd ed.; Marcel Dekker: New York, 1986.
(9) Hunter, R. J. *Foundations of Colloid Science*; Oxford University Press: London, 1989; Vol. I.
(10) Moon, P.; Spencer, D. E. *J. Franklin Inst.* **1992**, *255*, 374.
(11) Moon, P.; Spencer, D. E. *Field Theory Handbook*; Springer-Verlag: Berlin, 1961.
(12) Churchill, R. V.; Brown, J. W. *Complex Variables and Applications*; 5th ed.; McGraw-Hill: New York, 1984.
(13) Greenberg, M. D. *Application of Green's Functions in Science and Engineering*; Prentice-Hall: Englewood Cliffs, NJ, 1971.
(14) Hildebrand, F. B. *Methods of Applied Mathematics*, 2nd ed.; Prentice-Hall: Englewood, Cliffs, NJ, 1965.
(15) Verwey, E. J. W.; Overbeek, J. Th. G. *Theory of the Stability of Lyophobic Colloids*; Elsevier: Amsterdam, 1948.
(16) Bell, G. M.; Levine, S. *Trans. Faraday Soc.* **1958**, *54*, 785.
(17) Bell, G. M.; Levine, S.; McCartney, L. N. *J. Colloid Interface Sci.* **1970**, *33*, 335.